Thickness variation study of RFID-based folded patch antennas for strain sensing

Xiaohua Yi [a], Terence Wu [b], Gabriel Lantz [a], Yang Wang [a]*, Roberto T. Leon [a], and Manos M. Tentzeris [b]

[a] School of Civil and Environmental Eng., Georgia Inst. of Technology, Atlanta, GA 30332, USA
[b] School of Electrical and Computer Eng., Georgia Inst. of Technology, Atlanta, GA 30332, USA

ABSTRACT

This paper explores folded patch antennas for the development of low-cost and wireless smart-skin sensors that monitor the strain in metallic structures. When the patch antenna is under strain/deformation, its resonance frequency varies accordingly. The variation can be easily interrogated and recorded by a wireless reader that also provides power for the antenna operation. The patch antenna adopts a specially selected substrate material with low dielectric constant, as well as an inexpensive off-the-shelf radiofrequency identification (RFID) chip for signal modulation. A thicker substrate increases RFID signal-to-noise ratio, but reduces the strain transfer efficiency. To experimentally study the effect of substrate thickness, two prototype folded patch antennas with different substrate thicknesses have been designed and manufactured. For both prototypes, tensile testing results show strong linearity between the interrogated resonance frequency and the strain experienced by the antenna. Longer interrogation range is achieved with the larger substrate thickness.

Keywords: passive wireless sensor; folded patch antenna; strain sensor; substrate thickness; RFID

1. INTRODUCTION

Nearly one third of the 600,000 bridges in the U.S. are steel bridges, among which over one third are rated as structural deficient or functionally obsolete [1]. For all deficient bridges, fatigue-induced fracture/crack is among the most common concerns for inspectors and owners [2]. Early detection of crack is important, since the crack growth may lead to expensive repairs or cause catastrophic failures. The current biennial bridge inspection mandated by Federal Highway Administration (FHWA) is primarily a visual activity [3]. Small-size cracks or cracks hidden under paint easily remain elusive to human eyes; the cracks may grow to critical and dangerous sizes before the next inspection cycle. Early detection of cracks for fracture-critical-members of steel bridges has long been a challenging issue in bridge health monitoring. Some current technologies, including metal foil strain gages, fiber optic sensors, or ultrasonic testing, may assist in crack monitoring. However, current sensing systems either require running lengthy cables in the structure [4], or cover only very limited areas of the structure, or involve human-operated equipment that is not convenient for in-situ continuous application. As a result, these technologies suffer from their high instrumentation and monitoring cost and are not practical for large-scale/large-area deployment and continuous monitoring in the field.

Among many new technologies developed for structural health monitoring (SHM), wireless sensing has been widely explored in recent years [5-8]. Compared with conventional cable-based systems, wireless systems have the advantage of significantly reducing instrumentation time and cost. A comprehensive review on wireless sensing for SHM can be found in [9], which summarizes various academic and industrial wireless sensing devices that have been developed. The device usually contains an analog-to-digital converter for data sampling, a microprocessor for data processing and a wireless transceiver for communication. Most of these devices operate on batteries and acquire data from associated traditional sensors. For example, strain measurement can be achieved by interfacing the wireless device with a metal foil strain gage, acceleration measurement can be achieved by interfacing the device with a MEMS (micro-electro-mechanical systems) accelerometer, etc. Overall, wireless technology is primarily utilized to transmit the digitized sensor

* yang.wang@ce.gatech.edu; phone 1 404 894-1851; fax 1 404 894-2278; http://www.ce.gatech.edu/~ywang

data.

This research explores a different approach of exploiting wireless electromagnetic waves for strain sensing through the development of "smart skins" made of radiofrequency identification (RFID)-enabled patch antennas. Instead of using wireless technologies to transmit digitized data, the strain-dependent behavior of the electromagnetic waves in the antenna is exploited as the sensing mechanism. The basic concept is that when a small piece of electric antenna (usually with 2D shape) is under strain/deformation, its electromagnetic resonance frequency may change accordingly. Such change can be interrogated by a wireless reader and used as the strain indicator. Jia *et al.* [10] and Loh *et al.* [11] developed inductively coupled wireless strain sensors to measure the shift of resonance frequency under tensile strain. The experimental results showed linearity between the resonance frequency shift and the strain. Andringa *et al.* [12] and Chen *et al.* [13] successfully developed corrosion sensors using the same inductive coupling concept. One drawback of inductively coupled sensors, however, is that the interrogation distance is usually limited, i.e. at a level around 10cm.

To overcome the limitations in interrogation distance, electromagnetic backscattering systems can provide an alternative [14]. Tata *et al.* [15] and Deshmukh and Huang [16] developed a microstrip patch antenna for measuring strain and detecting cracks in metallic structures. The unique sensor design operates with a specially-devised light-activated radio-frequency (RF) switch, which requires an external circuit for the pseudomorphic high electron mobility transistor (pHEMT). The sensor operation also requires direct line-of-sight for passing the switching light beam. In addition, Chuang *et al.* [17] and Thomson *et al.* [18] developed a wireless strain sensor based on RF cavity, i.e. a metallic cylinder containing the strain sensing element inside. The RF cavity sensor achieved an interrogation distance of 8m [18]. Different from others' work that utilize a 2D antenna as the strain sensing element, the system requires an external regular antenna being connected outside the cavity at the sensor side. Meanwhile, the cavity-based sensor can be more suitable for embedment inside concrete, but not for surface installation on a steel plate. More recently, Yi *et al.* [19] developed a RFID-based folded patch antenna as a passive wireless strain sensor for metallic structures. The system utilizes the principle of electromagnetic backscattering and adopts a low-cost off-the-shelf RFID chip to reduce the design and manufacturing cost. The RFID-based technology allows the sensor to be passive, i.e. to operate without other power source such as batteries [20]. A special poly-tetra-fluoro-ethylene (PTFE) material with low dielectric constant is chosen as the antenna substrate, in order to improve the interrogation range by enhancing of the antenna quality factor. Through experiments, the strain sensing resolution is demonstrated to be under $50\mu\varepsilon$, and the wireless interrogation distance is shown to be over a few feet for this preliminary prototype.

In this research, two different substrate thicknesses are adopted to investigate the thickness effects on sensing performance. Since the thickness of the sensor substrate is relatively large compared with conventional metal foil strain gages, experiments are first performed to investigate the strain transfer efficiency. Tensile tests are then conducted to investigate the strain sensing performance of the prototype wireless sensors. Finally, the interrogation ranges of the two prototype wireless sensors are investigated. The rest of the paper is organized as follows. Section 2 first introduces the design and manufacturing of the two wireless strain sensors, followed by the operation principle of the system. Section 3 presents the strain transfer experiments. Section 4 describes the experimental results from tensile tests and interrogation range tests for the two prototype wireless sensors. Section 5 provides a summary and discussion of this work.

2. STRAIN SENSING PRINCIPLE

The wireless strain sensing system consists of an RFID reader and an RFID tag (i.e. wireless strain sensor), where the tag includes an antenna and an integrated circuit (IC) chip (Fig. 1). The operation of the system is based on the backscattering mechanism. The reader emits interrogation electromagnetic wave to the tag at power level P_1. Then the tag is activated and reflects wave back to the reader at power level P_2. Section 2.1 introduces the RFID tag design and the basic formulation for its resonance frequency. Section 2.2 describes how to extract the resonance frequency from the reader measurement.

2.1 RFID tag design

RFID tag designs are based on RFID IC chips that usually have very small feature sizes and are inexpensive to produce. The functions of an IC chip include: (1) harvesting the electromagnetic power from the interrogation signal emitted by the reader; (2) modulating the backscattered electromagnetic signal so that the signal can be properly recognized by the reader; (3) storing a small amount of data that can be accessed and modified by the RFID reader. Although the third
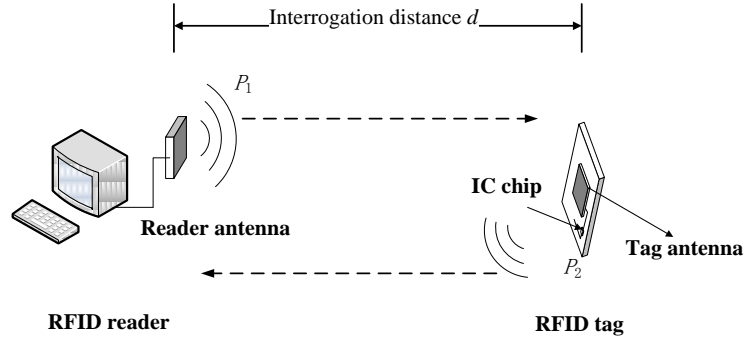
Fig. 1. Power transmission and backscattering in a passive RFID tag-reader system

function is currently not exploited, it can be explored in the future for storing historic strain measurement data in the RFID tag.

The RFID IC chip for this application is chosen as the SL3ICS1002 model from NXP Semiconductors. The impedance of the chip is $13.3\text{-}j122$ Ω ("j" is the imaginary unit), which is low and relatively easy to match during the tag antenna design. In addition, reliable operation of multiple tags can be achieved through advanced anti-collision mechanism, which allows the reader to simultaneously access multiple RFID tags within the neighborhood. The broad operating frequency range of the chip (from 840 MHz to 960 MHz) allows international usage.

The design drawing and picture of the Prototype A are shown in Fig. 2. Both the drawing and the picture illustrate the front/top side of the RFID tag, where the copper cladding (as the conducting component of the tag antenna) and IC chip are mounted on a 2.4 x 2.72 in. substrate. The back/bottom side of the tag is the electronic ground plane (also made of copper cladding) located on the back of the substrate. The thickness of the copper cladding at both sides of the substrate is 0.7 mils (0.0178 mm). The substrate material is Rogers RT/duroid®5880, a glass microfiber reinforced poly-tetra-
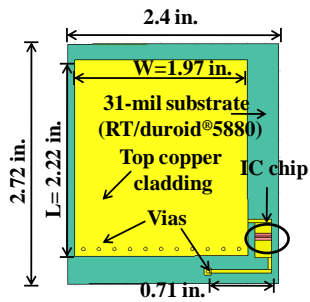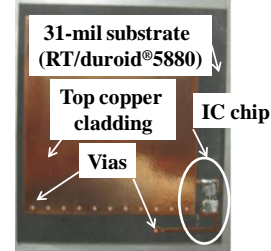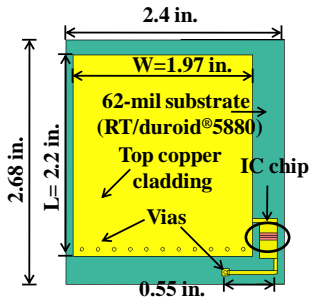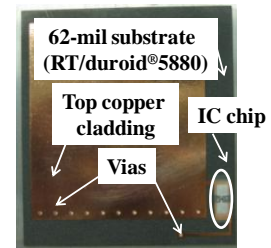

(a) Design drawing   (b) Picture of the manufactured tag

Fig. 2. RFID tag as wireless strain sensor (Prototype A)

(a) Design drawing   (b) Picture of the manufactured tag

Fig. 3. RFID tag as wireless strain sensor (Prototype B)

fluoro-ethylene (PTFE) composite with a dielectric constant ε_r of 2.20 and a thickness of 31 mils (0.79 mm). The RT/duroid®5880 material is adopted due to its low dielectric attenuation, which improves the interrogation range and the quality factor of the RFID tag. Prototype B with a thicker substrate is also designed for comparison, as shown in Fig. 3. Theoretically, a thicker substrate enables a longer interrogation range, but reduces the strain transferred through the substrate (i.e. from the surface of the underlying metallic structure, where the back-side copper cladding is bonded on, to the front-side copper cladding). This balance is considered and compared between the two prototype designs. The dimensions of the top copper cladding are similar for the two prototypes, except that the length of the top copper cladding for Prototype B is slightly shorter, and the length of the matching line is reduced from 0.71 in. to 0.55 in. Vias through the substrate are used at both prototypes for connecting the top copper cladding with the ground plane on the back of the substrate, as well as connecting one pin of the IC chip with the ground plane.

The RFID tag design is based on a quarter-wave rectangular patch antenna (folded-patch) topology [14]. The topology is chosen for its good radiation performance on top of metallic objects, and because it enables 50% reduction to the footprint of a regular patch antenna. The antenna resonance frequency at zero strain level, f_{R0}, can be estimated as:

$$f_{R0} = \frac{c}{4(L+\Delta L)\sqrt{\varepsilon_r}}$$

(1)

where c is the speed of light, L is the physical length of the top copper cladding (2.22 in. for Prototype A and 2.2 in. for Prototype B), ε_r is the dielectric constant of the substrate (2.20 for Rogers RT/duroid®5880), ΔL is the additional electrical length compensating the fringing effect. When the antenna experiences strain deformation of ε in the longitudinal direction, the shifted resonance frequency becomes:

$$f_R = \frac{c}{4(1+\varepsilon)(L+\Delta L)\sqrt{\varepsilon_r}} = \frac{f_{R0}}{1+\varepsilon}$$

(2)

When strain ε is small, the resonance frequency changes approximately linearly with respect to strain:

$$f_R \approx f_{R0}(1-\varepsilon)$$

(3)

This linear relationship indicates that by measuring the antenna resonance frequency, the applied strain can be derived.

2.2 Measurement of resonance frequency

The RFID reader (Fig. 1) adopted in this application is the Tagformance unit from Voyantic. The reader can sweep through an interrogation frequency range from 800 MHz to 1000 MHz. At each interrogation frequency, the reader emits different levels of power in order to find the transmitted power threshold (least transmitted power required to activate the IC chip). At default factory setting, the transmitted power threshold $P_1(f)$ plot provided by the reader can achieve 0.1 MHz resolution in frequency sweeping and 0.1dBm resolution in power measurement. Through a USB 2.0 port, a computer interface is used to operate and retrieve measurement data from the reader.

The RFID tag antenna has been designed such that when the interrogation frequency f is equal to the resonance frequency of the RFID tag, best impedance matching between the tag antenna and the IC chip occurs. At this time, the least amount of power needs to be transmitted by the reader for activating the RFID tag, which means the transmitted power threshold plot $P_1(f)$ (measured by the reader) reaches minimum value at the resonance frequency. When there is no strain/deformation, the minimum occurs at resonance frequency f_{R0} (Eq. (1)). When the antenna size changes due to strain ε, the resonance frequency changes accordingly to f_R (Eq. (2)), and the $P_1(f)$ plot for the antenna under strain reaches minimum at f_R.

3. STRAIN TRANSFER VALIDATION

Fig. 4 illustrates the RFID tag mounted at the center of an aluminum specimen under tension. The wireless strain sensing performance is expected to be the same for either aluminum or steel, since both materials are good metallic conductors. Aluminum specimens are used for tensile testing because they are much easier to machine than steel specimens. As described in Section 2.1, the sensing component of the RFID tag is the antenna, which consists of two layers of 0.7 mils (0.0178 mm)-thick copper cladding located on the top and bottom surfaces of the substrate. The
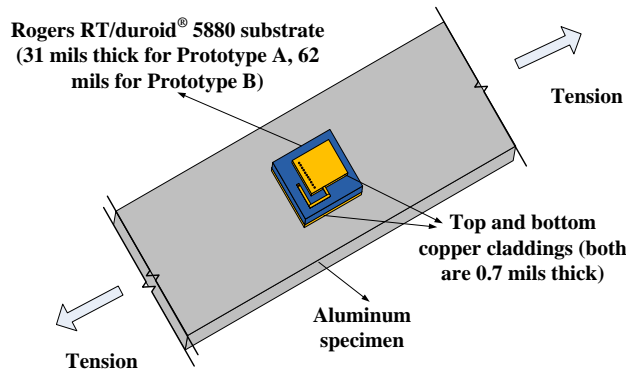
Fig. 4. RFID tag mounted at the center of an aluminum specimen (not to scale)

substrate thickness is 31 mils (0.79 mm) for Prototype A and 62mils (1.58 mm) for Prototype B. The copper cladding at the bottom surface is attached to the aluminum specimen using super glue from Super Glue Corporation. Experiments are conducted to verify that the stress/strain field in the tensile specimen is effectively transferred through the substrate to the top copper cladding, whose deformation ultimately causes the antenna resonance frequency change.

For the strain transfer experiments, two pieces of Rogers RT/duroid®5880 material with front and back copper claddings are prepared. One piece is 31 mils thick and has the similar size as Prototype A. The other piece is 62 mils thick and has the similar size as Prototype B. Fig. 5 is a picture taken for the center area of the testing specimen, showing eight metal foil strain gages (FLA-2-23-3LT, Texas Measurements, Inc) installed. Three strain gages (#1~#3) are installed directly on the aluminum along the loading direction, for measuring the axial strain. Another five strain gages (#4~#8) are installed on top of the RFID tag, for measuring the axial strain transferred to the top copper cladding. A National Instruments strain gage module (NI 9235), in combination with a CompactDAQ Chassis (NI cDAQ-9172) is used for collecting strain gage data. Tensile testing is conducted using a 22-kip SATEC machine.

Fig. 6(a) shows the strain data from the substrate piece with 31-mil thickness (simulating Prototype A). Starting from zero strain to 450 με, ten strain levels are measured at increments of approximately 50 με. For every data point, the horizontal-axis value is the average measurement among strain gages #1~#3; the vertical-axis value is the corresponding average measurement among gages #4~#8. A 45-degree reference line is drawn on the plot. At each strain level, the difference between horizontal and vertical-axis values is relatively small. Fig. 6(b) shows the percentage of the strain transferred from the aluminum specimen to the copper cladding, calculated as the ratio of the vertical-axis value over the horizontal-axis value for each data point in Fig. 6(a). The strain transfer percentage varies from 85.5% to 91%.

Similarly, the comparison between the strain on the specimen and on the top copper cladding for the substrate piece with 62-mil thickness (simulating Prototype B) at different strain levels are shown in Fig. 7. For the 62-mil piece, due to the
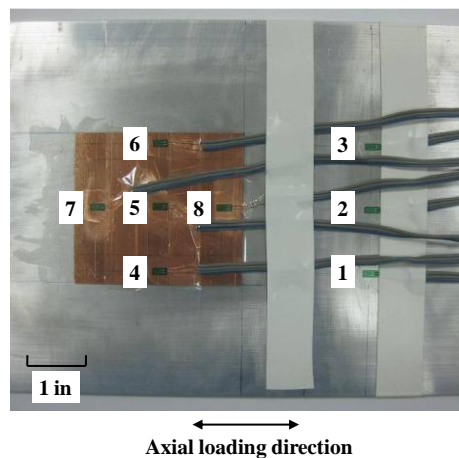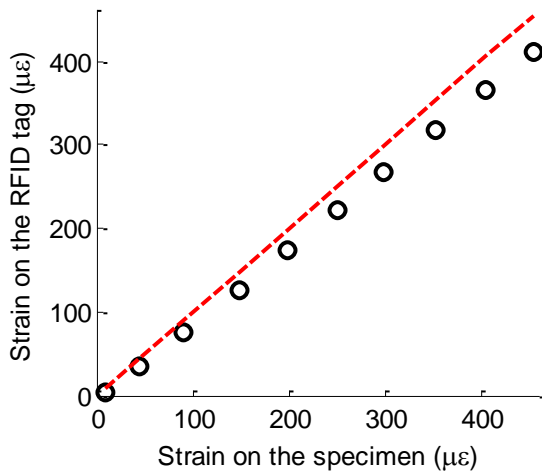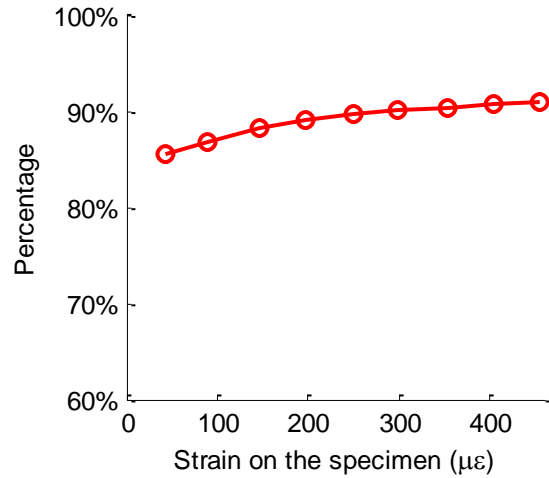

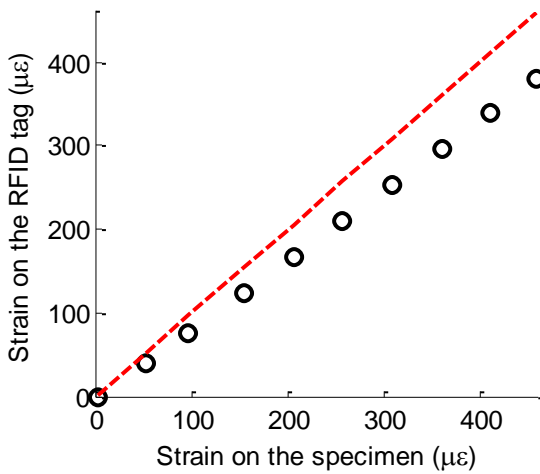Fig. 5. Picture of the validation experiments for strain transfer

(a) Average strain on the RFID tag vs. average strain on the aluminum specimen (the dashed line is a 45 °reference line)
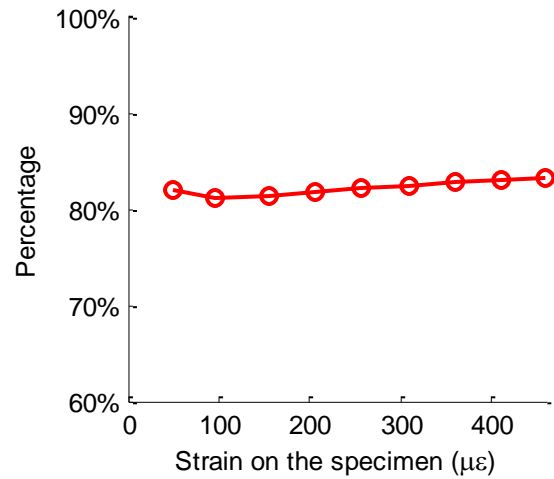
(b) Strain transfer percentage for different strain levels

Fig. 6. Experimental results for strain transfer (Prototype A)

(a) Average strain on the RFID tag vs. average strain on the aluminum specimen (the dashed line is a 45 °reference line)

(b) Strain transfer percentage for different strain levels

Fig. 7. Experimental results for strain transfer (Prototype B)

larger thickness, the strain transfer percentage reduces to 81% ~ 83%. These results illustrate for both prototypes, an adequate amount of strain is transferred from the aluminum to the top copper cladding, which can enable a corresponding resonance frequency shift in the wireless strain sensor. The small variation in strain transfer percentage at different strain levels is likely due to the effect of the superglue nonlinearity, coupled by the relatively large area that the superglue needs to be applied.

4. WIRELESS STRAIN SENSING EXPERIMENTS

The strain sensing performance of Prototype A has been validated and presented in [19]. The distance between the wireless strain sensor and the reader antenna was set to 12 in., and the sensing results demonstrated good linearity at 50με resolution. Similarly, in this study, Fig. 8(a) shows the center area of the tensile testing specimen, with the wireless strain sensor (Prototype A or B) and seven conventional strain gages (FLA-2-23-3LT, Texas Measurements, Inc) measuring the axial strain on the aluminum specimen. Fig. 8(b) shows the experimental setup for the tensile testing with
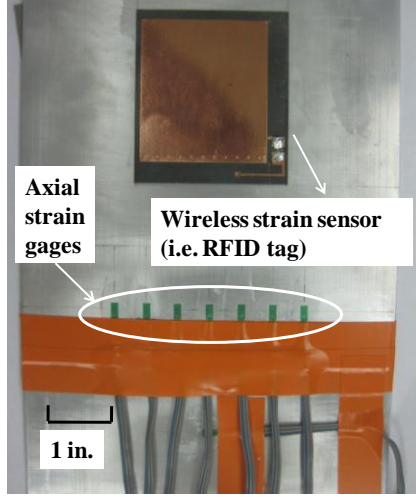
(a) Picture of the sensor instrumentation for wireless sensing experiments
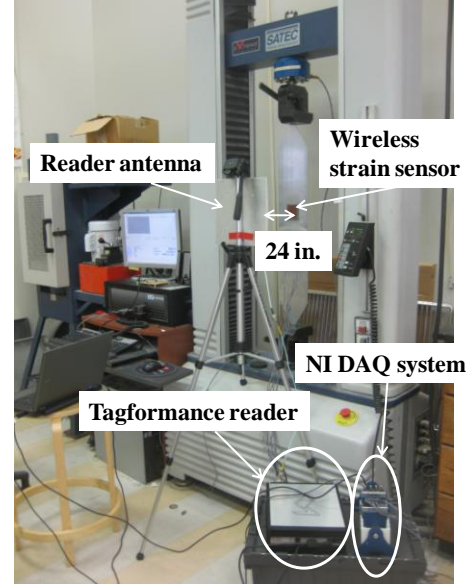
(b) Picture of the experimental setup

Fig. 8. Experimental setup for the tensile tests

a 22-kip SATEC machine. The reader antenna is mounted on a tripod facing the wireless strain sensor. The distance between the reader antenna and the wireless sensor is investigated to 24 in., in order to study whether thicker substrate improves performance at larger interrogation distance. Through a coaxial cable, the reader antenna is connected with the Tagformance reader, which communicates with a laptop through USB 2.0. A National Instruments strain gage module (NI 9235), in combination with a CompactDAQ Chassis (NI cDAQ-9172), is used for collecting data from conventional strain gages.

4.1 Strain sensing analysis

The force applied by the testing machine is configured so that approximately a 50με increment is achieved at each loading step. The average interrogation power threshold in dBm scale, $\underline{P}_1(f)$, is measured by the Tagformance reader at each loading step. Assuming P_1 is the power threshold in mW, the conversion to dBm scale is defined as:

$$\underline{P}_1 = 10\log_{10} P_1 \tag{4}$$

To reduce the effect of measurement noise, ten measurements are taken for each strain level and the average is calculated at every interrogation frequency f:

$$\bar{P}_1(f) = \frac{1}{10}\sum_{i=1}^{10}\left[\underline{P}_1^i(f)\right] \tag{5}$$

where $\bar{P}_1$ is the average transmitted power threshold in dBm, $\underline{P}_1^i(f)$ is the transmitted power threshold in dBm from the ith measurement. For example, the average transmitted power threshold at zero strain level is plotted as the solid line in Fig. 9(a). As described in Section 2.2, the transmitted power threshold reaches its minimum value at the resonance frequency. Since the valley area of the plot is relatively flat, the precise resonance frequency is not obvious. To resolve this difficulty, a 4th order polynomial curve fitting is performed to the valley area. The value of the fitted 4th order polynomial is re-calculated at a frequency step of 0.001MHz for identifying the resonance frequency.

Fig. 9(a) also shows the average transmitted power threshold plot, $\bar{P}_1(f)$, for other different strain levels. The strain levels are calculated as the average among the seven axial strain gages (Fig. 9(a)) and then corrected by the strain transfer percentages shown in Fig. 6. The resonance frequency f_R, as determined through the 4th order curve fitting, is plotted in Fig. 9(b) against the strain level, and linear regression is conducted to the seven data points. The slope

coefficient, -0.000793 MHz/με (i.e. -793 Hz/με), is the strain sensitivity of the wireless sensor, which means that 1 με increment causes 793 Hz decrease in the resonance frequency of the wireless strain sensor. As described in Section 2.1, the theoretical resonance frequency of the sensor at zero strain level is 920.8 MHz. The relative difference between the theoretical and the experimental resonance frequency f_{R0} is only 0.1%, which shows a very close match. In addition, according to Eq. (2), the theoretical strain sensitivity is -920.8 Hz/με. The difference between the analytical and experimental strain sensitivities is probably because the dielectric constant ε_r (which is assumed constant in the analytical study) changes with respect to strain. Different from an ideal material, small voids always exist in the substrate. Distortion of the voids under strain can affect the dielectric constant. The ε_r change due to strain requires in-depth studies in the future. Fig. 9(b) also shows the coefficient of determination, R^2, from the linear regression [21]. A value of $R^2 = 0.9864$ indicates an acceptable level of linearity. Nevertheless, although the determination coefficient R^2 is as high as 0.9984 for Prototype A at 12 in. interrogation distance [19], the linearity of Prototype A deteriorates at 24in.

Prototype B is tested using the same procedures, and the average transmitted power at different strain levels is plotted in Fig. 10(a). The resonance frequencies at these strain levels are extracted and plotted in Fig. 10(b). For Prototype B, the strain sensitivity is -0.000733 MHz (i.e. -733 Hz/με), which is close to the strain sensitivity of Prototype A. The determination coefficient R^2 for Prototype B is 0.9981, which indicates a better linearity than Prototype A at 24 in.
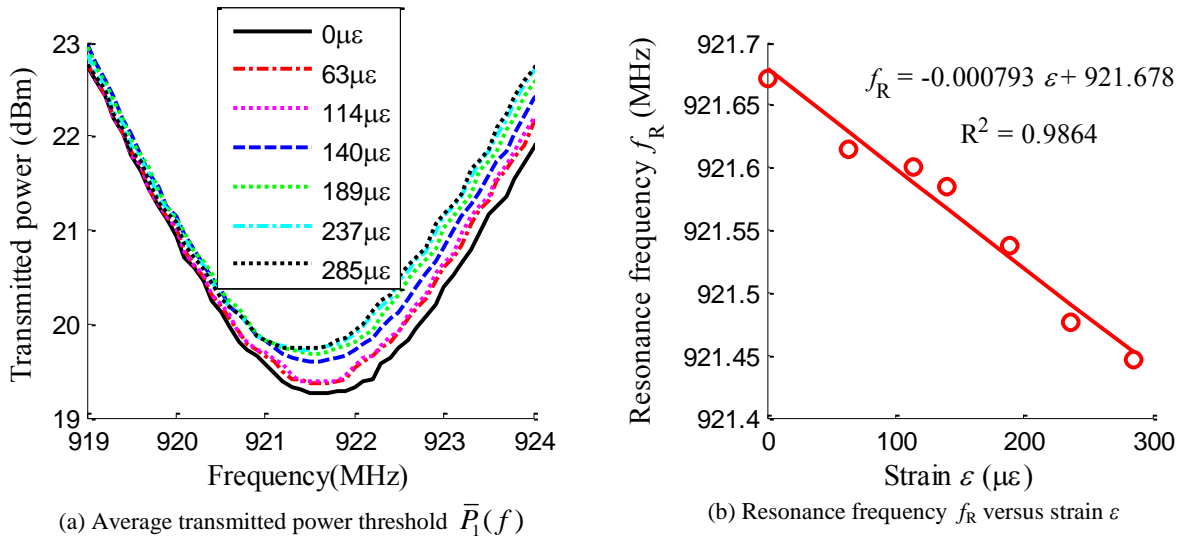
(a) Average transmitted power threshold $\overline{P}_1(f)$

(b) Resonance frequency f_R versus strain ε

Fig. 9. Tensile testing results for the ~50 με/step loading case at 24 in. interrogation distance (Prototype A)

(a) Average transmitted power threshold $\overline{P}_1(f)$
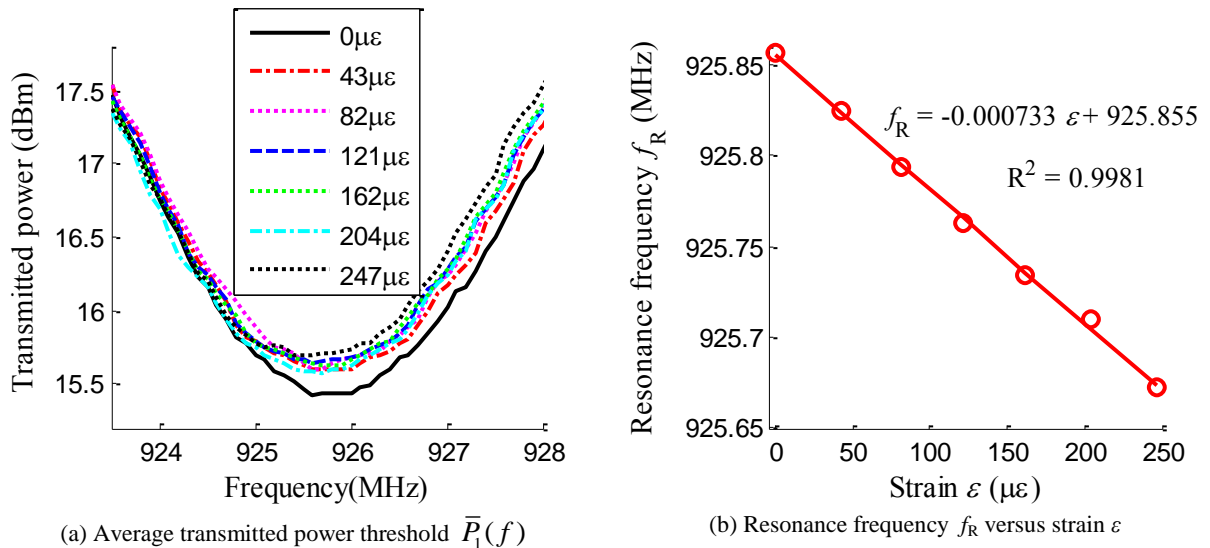
(b) Resonance frequency f_R versus strain ε

Fig. 10. Tensile testing results for the ~50 με/step loading case at 24 in. interrogation distance (Prototype B)

interrogation distance. The performance is expected because the quality factor of the patch antenna increases with a thicker substrate, allowing better performance at a relatively longer interrogation distance.

4.2 Strain sensing analysis

In order to investigate the largest interrogation distance that the prototype wireless sensors can provide, the sensors (Prototype A and B) under zero strain were tested with various interrogation distances. The experimental setup for the interrogation distance is shown in Fig. 11. Fig. 12(a) shows the average transmitted power threshold $\bar{P}_1(f)$ plots at different distances measured for Prototype A, and the distance varies from 12 in. to 50in. Fig. 12(b) shows the plots for Prototype B, and the distance varies from 12 in. to a maximum of 70 in.

While Prototype B provides similar sensitivity with Prototype A, the interrogation range of Prototype B is increased from 50 in. to 70 in. This coincides with the better linearity provided by Prototype B at 24 in. distance tensile testing. The resonance frequencies at different distances are extracted and plotted in Fig. 13. The variation for Prototype A is about 0.08 MHz, except for the 50 in. case. The variation of resonance frequencies for Prototype B is similar to that of Prototype A, except for the 60 in. case. The resonance frequency difference can be due to the multipath propagation of the electromagnetic wave, as well as environmental noise. It should be noted that regardless of the resonance frequency variation at different interrogation distances, wireless strain sensing is feasible as long as the relationship between the strain and the resonance frequency remains approximately linear at a fixed interrogation distance. Nevertheless, future
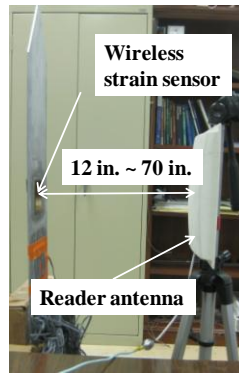

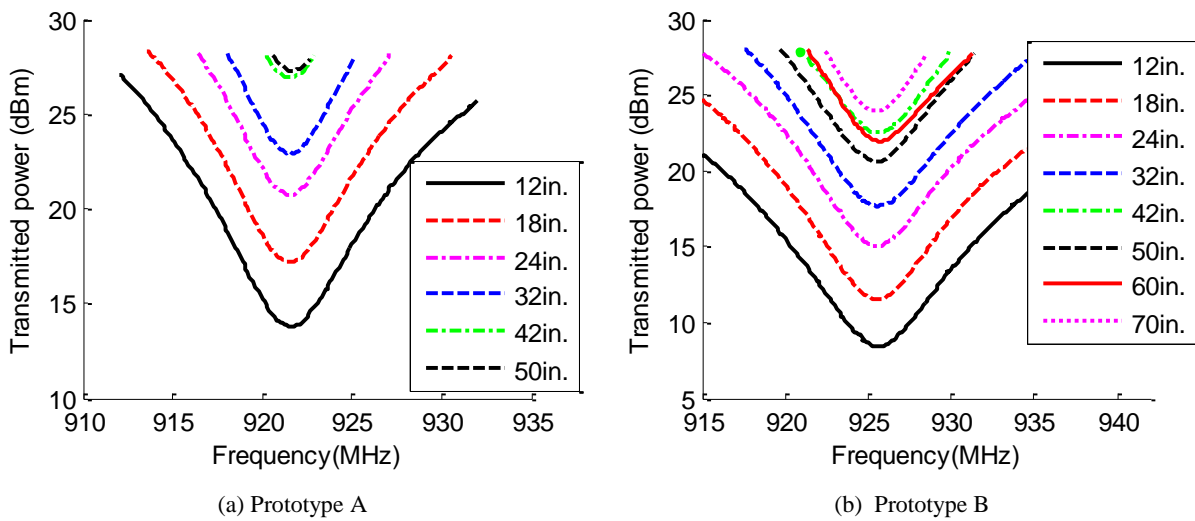Fig. 11. Experimental setup for the interrogation distance analysis

(a) Prototype A

(b) Prototype B

Fig. 12. Average transmitted power threshold plots (at zero strain level) for different interrogation distances
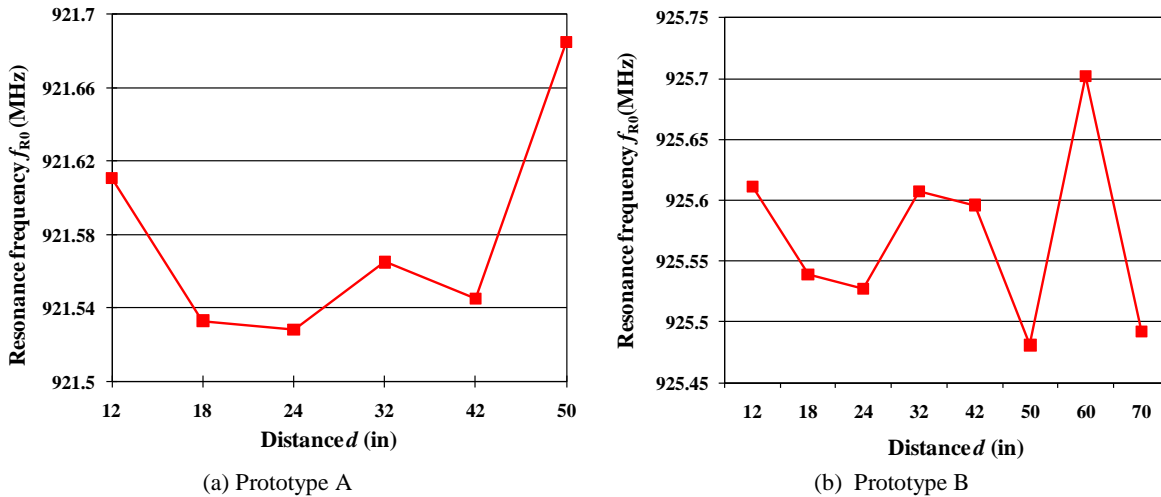
(a) Prototype A　　　　　　　　　　　　(b) Prototype B

Fig. 13 Resonance frequency f_{R0} (at zero strain level) extracted from the transmitted power threshold plots in Fig. 12

research will continue exploring advanced design, interrogation, or analysis techniques for more constant resonance frequencies at different interrogation distances.

5. SUMMARY AND DISCUSSION

This paper presents some preliminary investigation on the thickness effect of RFID-based passive wireless strain sensors utilizing folded patch antennas. Both analytical studies and tensile testing experiments demonstrate an approximately linear relationship between the resonance frequency of the antenna and the strain experienced by the sensor. It is shown that thicker substrate in Prototype B can improve the interrogation distance compared with thinner substrate in Prototype A. If the measurement result is calibrated using the strain transfer percentage, the two prototype sensors have similar strain sensitivities. Not requiring battery power, the low-cost passive wireless strain sensor has the potential to offer large-scale dense deployment for civil structures. Although compared with traditional metal foil strain gages, the measurement precision of this preliminary prototype is yet to be improved, the operational convenience enabled by the wireless/batteryless sensor may outweigh the disadvantage, particularly for scenarios where qualitative (rather than quantitative) measurements are sufficient.

Since the resonance frequency of the wireless strain sensor is correlated with the size of the patch antenna, the footprint of the sensor can be significantly reduced in future studies by increasing the operating frequency. In addition, longer interrogation distance can be achieved by adopting a high gain antenna at the reader side, and the consistency of the resonance frequency at various distances deserves further investigation.

ACKNOWLEDGEMENT

REFERENCES

[1] FHWA, *National Bridge Inventory*. U.S. Department of Transportation, Federal Highway Administration, Washington D.C. (2011).

[2] ASCE, *Report Card for America's Infrastructure*. American Society of Civil Engineers, Reston, VA (2009).

[3] AASHTO, *Manual of Bridge Evaluation*. American Association of State Highway & Transportation Officials, Washington D.C. (2009).

[4] Çelebi, M., *Seismic Instrumentation of Buildings (with Emphasis on Federal Buildings)*. Report No. 0-7460-68170, United States Geological Survey, Menlo Park, CA (2002).

[5] Straser, E.G. and Kiremidjian, A.S., *A Modular, Wireless Damage Monitoring System for Structures*. Report No. 128, John A. Blume Earthquake Eng. Ctr., Stanford University, Stanford, CA (1998).

[6] Spencer, B.F., Jr., Ruiz-Sandoval, M.E. and Kurata, N., "Smart sensing technology: opportunities and challenges," *Struct. Control Hlth.*, 11(4), pp. 349-368 (2004).

[7] Lynch, J.P., Law, K.H., Kiremidjian, A.S., E., C., Farrar, C.R., Sohn, H., Allen, D.W., Nadler, B. and Wait, J.R., "Design and performance validation of a wireless sensing unit for structural health monitoring applications," *Struct. Eng. Mech.*, 17, pp. 393-408 (2004).

[8] Wang, Y., Lynch, J.P. and Law, K.H., "A wireless structural health monitoring system with multithreaded sensing devices: design and validation," *Struct. and Infrastructure Eng.*, 3(2), pp. 103-120 (2007).

[9] Lynch, J.P. and Loh, K.J., "A summary review of wireless sensors and sensor networks for structural health monitoring," *Shock Vib. Dig.*, 38(2), pp. 91-128 (2006).

[10] Jia, Y., Sun, K., Agosto, F.J. and Quinones, M.T., "Design and characterization of a passive wireless strain sensor," *Meas. Sci. Technol.*, 17(11), pp. 2869-2876 (2006).

[11] Loh, K.J., Lynch, J.P. and Kotov, N.A., "Inductively coupled nanocomposite wireless strain and pH sensors," *Smart Struct. Syst.*, 4(5), pp. 531-548 (2008).

[12] Andringa, M.M., Neikirk, D.P., Dickerson, N.P. and Wood, S.L., "Unpowered wireless corrosion sensor for steel reinforced concrete," *Proceedings of the IEEE sensors*, pp. 155-158, (2005).

[13] Chen, Y., Munukutla, S., Pasupathy, P., Neikirk, D.P. and Wood, S.L., "Magneto-inductive waveguide as a passive wireless sensor net for structural health monitoring," *Proc. SPIE*, 7647: 764749, (2010).

[14] Finkenzeller, K., *RFID Handbook*, Wiley, New York (2003).

[15] Tata, U., Huang, H., Carter, R.L. and Chiao, J.C., "Exploiting a patch antenna for strain measurements," *Meas. Sci. Technol.*, 20(1), 015201 (2009).

[16] Deshmukh, S. and Huang, H., "Wireless interrogation of passive antenna sensors," *Meas. Sci. Technol.*, 21(3), 035201 (2010).

[17] Chuang, J., Thomson, D.J. and Bridges, G.E., "Embeddable wireless strain sensor based on resonant RF cavities," *Rev. Sci. Instrum.*, 76(9), 094703 (2005).

[18] Thomson, D.J., Card, D. and Bridges, G.E., "RF cavity passive wireless sensors with time-domain gating-based interrogation for SHM of civil structures," *IEEE Sensors J.*, 9(11), pp. 1430-1438 (2009).

[19] Yi, X., Wu, T., Wang, Y., Leon, R.T., Tentzeris, M.M. and Lantz, G., "Passive wireless smart-skin sensor using RFID-based folded patch antennas," *Int. J. Smart Nano Mater.*, in print (2011).

[20] Balanis, C.A., *Antenna Theory: Analysis and Design*, John Wiley and Sons Inc., New York (1997).

[21] Chatterjee, S. and Hadi, A.S., "Influential observations, high leverage points, and outliers in linear regression," *Stat. Sci.*, 1(3), pp. 379-416 (1986).